RSC Advances

PAPER

View Article Online
View Journal | View Issue

Cite this: *RSC Adv.*, 2025, **15**, 15530

Synthesis, structural characterization, and DFT investigation of a mixed-valence Co(III)/Co(II) complex stabilized by supramolecular interactions†

Susovan Bera,[a] Sudip Bhunia,[a] Rosa M. Gomila,[b] Antonio Frontera[b] and Shouvik Chattopadhyay *[a]

A dinuclear mixed-valence cobalt(III/II) complex, $[(DMSO)(SCN)Co^{III}LCo^{II}(NCS)_2(OH^2)]\cdot DMF$, has been synthesized and structurally characterized by elemental analysis, spectroscopy, and single-crystal X-ray diffraction. The structure reveals a hexa-coordinated cobalt(III) center in an octahedral geometry and a penta-coordinated cobalt(II) center adopting a square pyramidal geometry. To support the oxidation state assignment, a spin density analysis was carried out, confirming spin localization on the cobalt(II) center. Additionally, a comprehensive DFT study was performed to evaluate key supramolecular interactions in the solid state. Theoretical analysis of selected assemblies using molecular electrostatic potential (MEP) mapping, QTAIM, and NCIplot methods reveals the energetic and directional features of dominant hydrogen bonds, including NH···S and OH···O interactions. The substantial interaction energies (up to −31.4 kcal mol^{-1}) and topological descriptors underscore the structure-directing role of these noncovalent contacts in the formation of one-dimensional supramolecular chains.

Received 8th April 2025
Accepted 30th April 2025

DOI: 10.1039/d5ra02432c

rsc.li/rsc-advances

Introduction

Polynuclear complexes of different transition and non-transition metals have attracted the interest of inorganic chemists and material scientists due to their amazing photo-catalytic and bio-mimicking catalytic activities, potential energy applications, ability to detect different trace elements and explosives, fascinating magnetic properties, applications in opto-electronics and medicinal chemistry, *etc.*[1–15] Among them, complexes of cobalt represent a unique class due to their ability to show SMM (single molecule magnet) and field induced SMM behaviors.[16–23] The use of cobalt complexes as catalysts for the oxidation of water to oxygen under sunlight thereby producing clean and sustainable energy is well established.[24–28] Schiff bases and their reduced analogues have also been used by several research groups to produce mixed valence complexes (containing both +II and +III oxidation states) of cobalt.[29–31] Most of the complexes are dinuclear or trinuclear, although tetranuclear complexes are also reported in literature.[32–41] The SMM behavior or field induced SMM behaviour of many di and trinuclear mixed valence cobalt(III/II) complexes with Schiff base or reduced Schiff base ligands is also reported in literature.[42,43] The complexes have also been used to fabricate different opto-electronic devices.[44–46] Many cobalt complexes were shown to have different bio-mimicking catalytic abilities, *e.g.* phosphatase mimicking activity (to catalyze the hydrolysis of (4-nitrophenyl)phosphate ester), catechol mimicking activity (to catalyze the aerial oxidation of 3,5-DTBC to 3,5-DTBQ (3,5-di-*tert*-butylbenzoquinone)), phenoxazinone synthase mimicking activity (to catalyze the aerial oxidation of *o*-aminophenol to 2-aminophenoxazine-3-one) *etc.*[47–52] Different non-covalent interactions, *e.g.* H-bonding, CH···π, π···π, cation···π, anion···π interactions *etc.* in the solid state structures of the complexes play an important role to grow different supramolecular architectures.[53–61] Crystal engineers, theoretical chemists and supramolecular chemists are interested to analyze different supramolecular structures in their solid state structures and like to estimate the energy of different interactions.[62–67]

In the present work, a reduced Schiff base ligand, (2,2-dimethyl-1,3-propanediyl)bis(iminomethylene)bis(phenol) (H_2L), was synthesized and employed to prepare a dinuclear, mixed-valence cobalt complex, $[(DMSO)(SCN)Co^{III}LCo^{II}(NCS)_2(OH_2)]\cdot DMF$. The complex has been fully characterized, including single-crystal X-ray diffraction analysis, which reveals distinct coordination environments for the cobalt(III) and cobalt(II) centers. To gain deeper insight into the electronic structure and the supramolecular organization in the solid state, we carried out a detailed theoretical study. Spin density mapping was used to confirm the oxidation state distribution, while molecular electrostatic potential (MEP) analysis, QTAIM,

[a]*Department of Chemistry, Inorganic Section, Jadavpur University, Kolkata 700032, India. E-mail: shouvik.chattopadhyay@jadavpuriuniversity.in; Tel: +91-33-24572941*
[b]*Departament de Química, Universitt de les Illes Balears, Crta de Valldemossa km 7.5, 07122 Palma de Mallorca, Baleares, Spain. E-mail: toni.frontera@uib.es*

† Electronic supplementary information (ESI) available: Fig. S1–S4 and Table S1. CCDC 2441974. For ESI and crystallographic data in CIF or other electronic format see DOI: https://doi.org/10.1039/d5ra02432c

and NCIplot methods were employed to elucidate the nature and strength of key intermolecular interactions.

In this context, our motivation was to synthesize and characterize a new dinuclear mixed-valence cobalt(III/II) complex stabilized by supramolecular interactions. Mixed-valence cobalt systems are of considerable interest due to their potential applications in catalysis, molecular magnetism, and materials science.[29,37,38] Moreover, studying the role of hydrogen bonding and other weak intermolecular interactions provides important insights into the supramolecular assembly of such complexes, which can be exploited to tailor functional properties. Although the present work is focused on fundamental structural and bonding aspects, the complex synthesized could serve as a promising candidate for future studies aimed at developing catalysts or molecular magnetic materials.

Experimental

Materials

The chemicals used for the synthesis of the complex were purchased from Sigma-Aldrich, India. No further purification of the materials was required prior to their use.

Caution! Although not encountered during experimental work, perchlorate salts of metal complexes with organic ligands are potentially explosive. Only a small amount of material should be prepared and it should be handled with care.

Synthesis of $[(DMSO)(SCN)Co^{III}LCo^{II}(NCS)_2(OH_2)]\cdot DMF$. A compartmental salen-type Schiff base ligand, {2,2′-[(2,2-dimethyl-1,3-propanediyl)bis(nitrilomethylidyne)]bis[phenol]}, was synthesized by refluxing 1,3-diaminopropane (∼1 mmol, 0.1 mL; purity: ≥99%) with 3-methoxysalicylaldehyde (∼2 mmol, 340 mg; purity: ≥99%) in methanolic solution (15 mL) for 1.3 h. Then the methanol (purity: ≥99%) solution was cooled in an ice-bath and then sodium borohydride (∼4 mmol, 150 mg; purity: ≥95%) was added to it slowly with constant stirring for 15 minutes. Then glacial acetic acid (2 mL, purity: ≥99%) was added to the resulting solution and stirred for another 10 minutes. The solution was evaporated to dryness under reduced pressure in a rotary evaporator (∼65 °C). The residue was dissolved in water (5 mL) and extracted with dichloromethane (5–8 mL, purity: ≥99%) using a separating funnel. Then, 10 mL of aqueous sodium bicarbonate (∼200 mg; purity: ≥99%) solution was added to neutralize extra acidic part in reaction medium. The organic phase was dried over anhydrous sodium acetate and the solvent *i.e.* dichloromethane was evaporated under reduced pressure using a rotary evaporator and the reduced Schiff base ligand, H_2L {(2,2-dimethyl-1,3-propanediyl)bis(iminomethylene)bis(phenol)}, was collected in methanol.

The methanolic solution of the dicondensed reduced Schiff base ligand H_2L (approximately 2 mmol), was then added to a 5 mL methanolic solution of $Co(ClO_4)_2\cdot 6H_2O$ (∼2 mmol, 730 mg; purity: ≥98%) and the resulting reaction mixture was stirred at room temperature for 1 h to produce a brown colour solution. Then 1 : 1 (v/v) methanol/water solution (∼5 mL) of sodium thiocyanate (80 mg, ∼1 mmol; purity: ≥98%) was added to the resulting solution followed by the dropwise addition of DMF (purity: ≥99%) with constant stirring for another 1 h then the reaction mixture was allowed to stand overnight. Dark single crystals of the complex started to appear at the bottom of the beaker within a few days and was collected by filtration and then dried in open atmosphere at room temperature.

The chemical composition was confirmed by elemental analyses (carbon, hydrogen and nitrogen) by using a PerkinElmer 240C elemental analyzer. IR spectrum in KBr (4500 to 500 cm^{-1}) was recorded with a PerkinElmer RX-1 FTIR. The electronic absorption spectrum (800–200 nm) in acetonitrile solution was collected using a SHIMADZU UV1900i, UV-vis spectrophotometer.

Yield: 464 mg (∼60%) based on Cobalt. Anal. Calc. for $C_{27}H_{39}Co_2N_6O_5S_4$ (FW: 773.78): C, 41.9; H, 5.08; N, 10.86. Found: C, 42.0; H, 5.1; N, 10.9%, FT-IR (KBr, cm^{-1}): 3411 (ν_{OH}), 3158 (ν_{N-H}), 2977–2932 (ν_{C-H}), 2071 (ν_{NCS}). UV-vis, λ_{max} (nm), [ε_{max} (L mol^{-1} cm^{-1})] (acetonitrile): 262 (1.6×10^4), 345 (7.1×10^3), 622 (0.82×10^3). Magnetic moment: 4.98 BM.

Crystal data: $C_{24}H_{32}Co_2N_5O_4S4$, C_3H_7NO; FW = 773.78; monoclinic space group $P2_1/n$, a = 14.7901(13) Å; b = 15.1095(12) Å; c = 16.3477(14) Å, β = 105.661(3), V = 3517.6(5) $Å^3$, Z = 4, D_{Calc} = 1.461 gm cm^{-3}, $F(000)$ = 1604, mu = 1.224 mm^{-1}. The data were collected at 273 K under the flow of liquid nitrogen using a 'Bruker D8 QUEST area detector' diffractometer equipped with graphite-monochromated Mo K_α radiation (λ = 0.71073 Å). Numbers of independent reflections = 7761. The molecular structure was solved by direct method and refined by full-matrix least squares on F^2 using SHELXL-97 to R_1 = 0.1303, wR_2 = 0.2126 using 50 550 reflections for the complex.[68] R(int) = 0.097, no. of parameters = 407. [$R_1 = \Sigma||F_o| - |F_c||/\Sigma|F_o|$, $wR_2 = \Sigma w(|F_o|^2 - |F_c|^2)^2/\Sigma w(|F_o|^2)^{1/2}$] non-hydrogen atoms were refined with anisotropic thermal parameters. The hydrogen atoms attached to nitrogen were located by difference Fourier maps and were kept at fixed positions. All other hydrogen atoms were placed in their geometrically idealized positions and constrained to ride on their parent atoms. Multi-scan empirical absorption corrections were applied to the data using the program SADABS.[69]

Hirshfeld surface analysis. Hirshfeld surface analysis was run to understand the structural flexibility and magnitude of interchain interactions.[70] Hirshfeld surface and associated 2D-fingerprint plots were calculated using Crystal Explorer.[71,72]

Theoretical calculations. The assemblies were computed using the PBE0-D4/def2-TZVP[73–75] level of theory and the Turbomole 7.7 program.[76] The interaction energies were computed by substracting the energy of the monomers to the energy of the assembly. The positions of the H-atoms involved in the H-bonding interactions were optimized. The topological analysis of the electron density was made according to QTAIM[77] and NCIplot[78] methods. These topological analyses were performed using the MultiWFN program[79] at the PBE0-D4/def2-TZVP level of theory.

The PBE0 hybrid functional was selected for all calculations because of its well-established performance in accurately predicting electronic structures, spin distributions, and non-covalent interaction energies in transition-metal complexes.[73] In particular, PBE0 is known to offer a balanced treatment of

exchange and correlation effects, which is critical for systems involving both localized and delocalized electronic features. The addition of the D4 dispersion[74] correction ensures a reliable description of noncovalent interactions, which are central to this study. Previous benchmarks have demonstrated the good accuracy of PBE0 for coordination compounds and supramolecular assemblies involving first-row transition metals.[80]

Results and discussion

Synthesis

The Schiff base and reduced Schiff base ligand {(2,2-dimethyl-1,3-propanediyl)bis(iminomethylene)bis(phenol) (H_2L)}, was synthesized following the reported method.[81–84] The reduced Schiff base ligand was then mixed with $Co(ClO_4)_2\cdot 6H_2O$ and sodium thiocyanate in methanol with constant stirring at room temperature to yield the complex. Synthetic route to the formation of the complex has been shown in Scheme 1.

Description of structure

[[(DMSO)(NCS)Co^{III}LCo^{II}(NCS)$_2$(OH$_2$)]](DMF)]. The single crystal X-ray structural analysis indicates that the complex crystallizes in the monoclinic, $P2_1/n$ space group. The structure of the complex is shown in Fig. 1 with the selective atomic numbering scheme. The oxidation states of Co(1) and Co(2) have been assigned as +III and +II respectively. Discrimination between cobalt(III) and cobalt(II) centers is based on bond length considerations.

Co(1) is equatorially coordinated by the two amine nitrogen atoms [N(1), N(2)] and two phenolate oxygen atoms [O(1), O(2)], from the tetradentate reduced Schiff base ligand. The axial positions are occupied by the thiocyanate nitrogen atom, N(3) and sulphur (S1) atom of coordinated solvent DMSO. On the other hand, Co(2) is equatorially coordinated by two phenolate oxygen atoms, [O(1), O(2)], two nitrogen atoms, N(4) and N(5) of two terminal thiocyanate groups and an oxygen atom [(O(4))] of a coordinated water molecule to complete its penta-coordinated square pyramidal geometry. Relatively large Co(1)···Co(2) distances {3.068(1) Å} are not indicative of any cobalt–cobalt bonding.[85–89] The thiocyanates are quasi-linear with the N–C–S angles being 178.9(6)°, 178.0(7)° and 177.6(6)°, as expected.[90] The saturated six-membered chelate ring [Co(1)–N(1)–C(8)–C(9)–C(12)–N(2)] has envelope conformation with the puckering parameters, $q = 0.548(6)$Å; $\theta = 12.05(5)°$; $\phi = 185(3)°$.[91,92]

Hirshfeld surface analysis

The Hirshfeld surface is mapped over d_{norm} (range ~0.1 Å to 1.5 Å), shape index and curvedness (Fig. S1†). Red spots on the Hirshfeld surfaces denote the dominant interactions. The intermolecular interactions appear as distinct spikes in the 2D fingerprint plot shows the different spikes with their corresponding interactions. The dominant interactions in the complex correspond to H···H/H···H (45%), C···H/H···C (16.8%), S···H/H···S (30.8%), O···H/H···O (3%) and N···H/H···N (2.6%) contacts. 2D fingerprint plot of the complex is shown in Fig. S2.†

IR and electronic spectroscopy study

The absence of any major band at around 1600 cm^{-1} (corresponding to azomethine bond) in the IR spectrum of the complex confirms the complete reduction of the azomethine group. A strong band for the terminal N-bonded thiocyanate group in complex is observed at 2071 cm^{-1}.[90] Broad bands in the range of 2859–3072 cm^{-1} may be attributed to the C–H stretching vibrations.[93–95] The band around 3158 cm^{-1} may be assigned to N–H stretching vibrations.[96] A distinct band is observed in the IR spectrum of the complex at 3411 cm^{-1} due to O–H stretching vibration.[97] The IR spectrum of this complex is given in Fig. S3.†

The complex shows intense absorption bands around 243–275 nm, which may be assigned as to n–π* transitions.[98] The band at *ca.* 345 nm may be attributed to a ligand-to-metal charge transfer transition (LMCT).[98,99] A band at 620 nm may be assigned as d–d transition.[95] The electronic spectrum of the complex in acetonitrile medium at room temperature in the range 200–900 nm is shown in Fig. S4.†

Electrochemical studies

Cyclic voltammetry of the complex (with 10^{-3} M solution in DMF) was performed a with glassy carbon as the working electrode, Ag/AgCl as the reference electrode, and platinum wire as the auxiliary electrode incorporating TBAB (tetrabutylammonium bromide) as supporting electrolytet 300 K in argon atmosphere. The potential range covered by the cyclic voltammetry was −2.0 V to +2.0 V. The scan rate was 150 mV s^{-1}.

The complex exhibits two one-electron responses, one of which is irreversible redox signal, and the other is quasi-

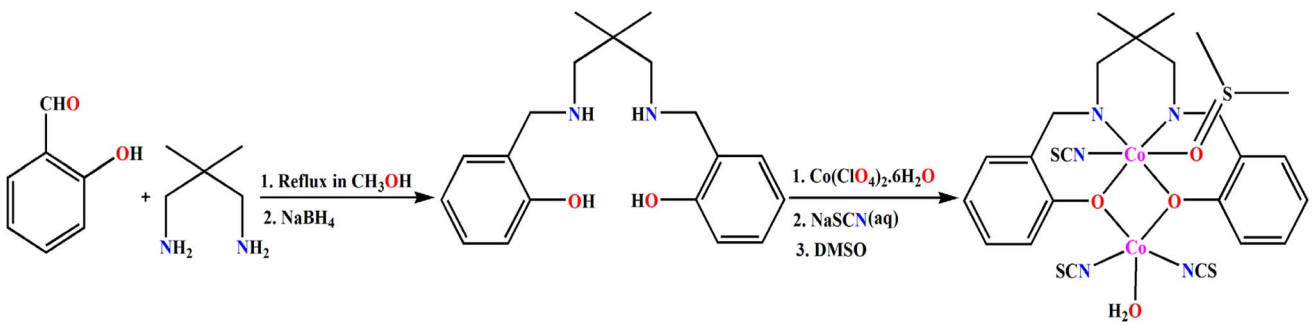

Scheme 1 Synthetic route to complex **1**.

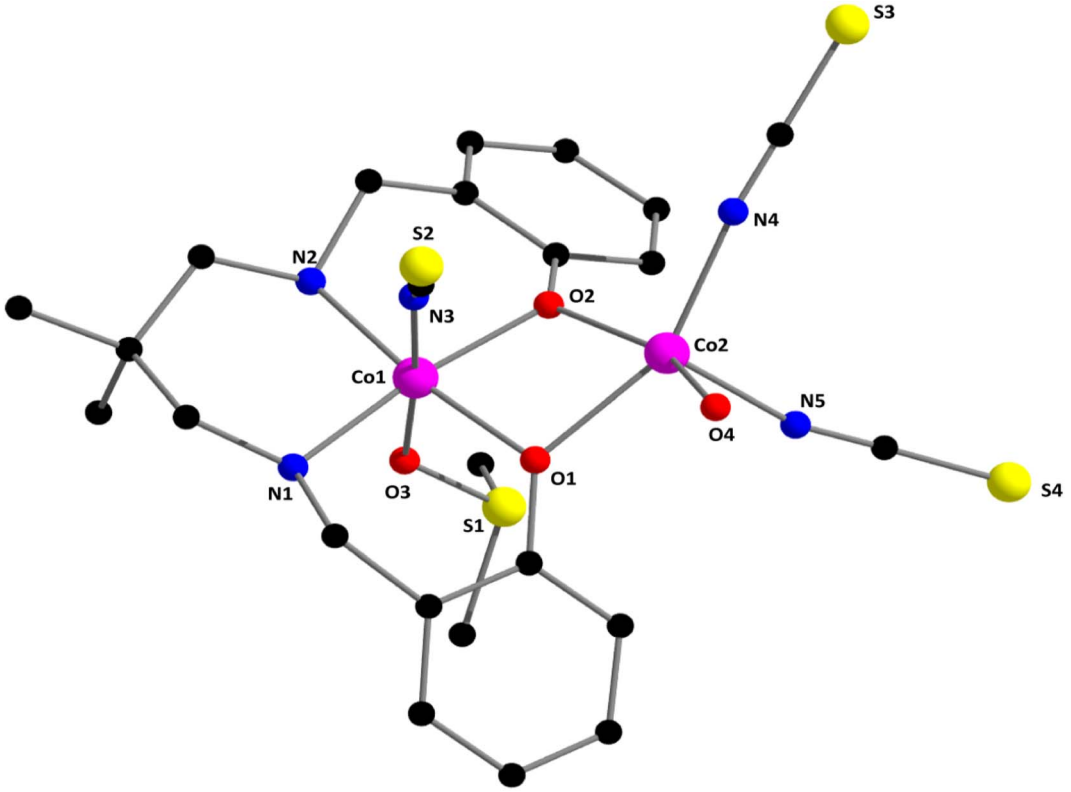

Fig. 1 Perspective view of complex **1** with selective atom numbering scheme. Selected bond lengths (Å): Co(1)–O(1) 1.927(3), Co(1)–O(2) 1.925(4), Co(1)–O(3) 1.923(5), Co(1)–N(1) 1.986(5), Co(1)–N(2) 1.975(5), Co(1)–N(3) 1.898(6), Co(2)–O(1) 2.077(4), Co(2)–O(2) 2.041(3), Co(2)–O(4) 2.095(5), Co(2)–N(4) 2.011(6), Co(2)–N(5) 2.018(6). Important angles have been listed in Table S1 (ESI).†

reversible (Fig. 2). The quasi-reversible redox signal consists of an oxidation peak, E_{pa} at +1.41 V and a reduction peak, E_{pc} at +1.31 V, whereas the irreversible signal consists only a reduction peak, E_{pc} at −0.66 V. The quasi-reversible redox signal may be attributed to the $Co^{II} \rightarrow Co^{III}$ oxidation and the $Co^{III} \rightarrow Co^{II}$ reduction, whereas the irreversible signal is attributed to the $Co^{III} \rightarrow Co^{II}$ reduction.[100,101] The detailed electrochemical data is given in Table 1.

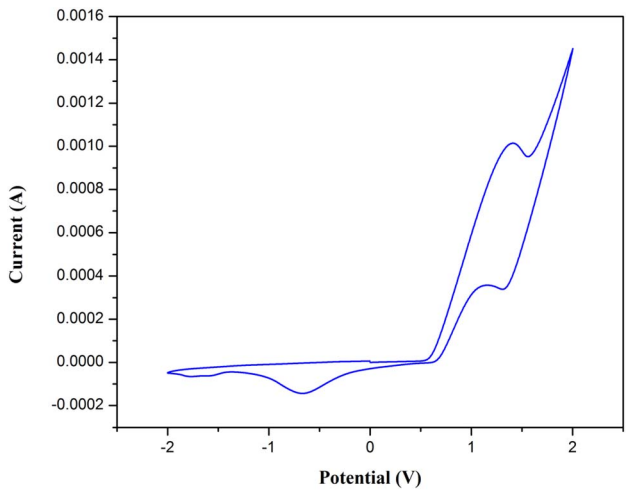

Fig. 2 Cyclic voltammogram of the complex in DMF (using Ag/AgCl reference electrode).

DFT calculations

The theoretical investigation began with a spin density analysis to support the assignment of the paramagnetic cobalt(II) center to the five-coordinate site, and the diamagnetic cobalt(III) ion to the octahedral site. As shown in Fig. 3, the spin density is predominantly localized on the cobalt(II) center (2.83 e), with minor delocalization onto the directly bonded atoms (0.15 e), and only a negligible residual spin density on the cobalt(III) center (0.02 e).

Next, we analyzed selected assemblies extracted from the solid-state structure of the complex to investigate the energetic characteristics of key hydrogen bonds (see Fig. 4). In particular, we focused on a supramolecular assembly in which two complexes are bridged by two DMF molecules, forming an $R_4^4(8)$ synthon (Fig. 4a). Additionally, two NH···S hydrogen bonds are established between the coordinated amino groups of one complex and the thiocyanate ligands of an adjacent complex, resulting in homodimeric assemblies (Fig. 4b). These dimers further propagate into one-dimensional supramolecular chains in the solid state. The DFT analysis aims to quantify these hydrogen bonds and is complemented by a combined QTAIM and NCIplot approach, as this combination is well suited to identifying real-space interactions and revealing their attractive nature.

To gain further insight, we computed the molecular electrostatic potential (MEP) surface of the complex to identify the

Table 1 Cyclic voltammetry data (V) for the complex in DMF medium[a]

Scan rate (mV s^{-1})	E_{pa} (V) ($Co^{II} \rightarrow Co^{III}$)	E_{pc} (V) ($Co^{III} \rightarrow Co^{II}$)	$E_{1/2}$ (V) ($Co^{II} \rightarrow Co^{III}$)	ΔE_p ($Co^{II} \rightarrow Co^{III}$)	E_{pc} (V) ($Co^{III} \rightarrow Co^{II}$)
150	+1.41	+1.31	+1.36	+0.10	−0.66

[a] $E_{1/2}$ denotes the half-wave potential. $E_{1/2} = (E_{pa} + E_{pc})/2$ and $\Delta E_p = (E_{pa} - E_{pc})$.

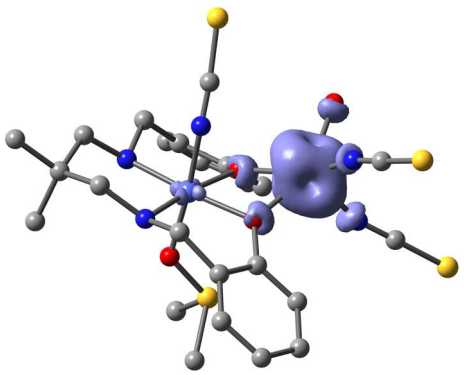

Fig. 3 Spin density plot of the complex (isovalue 0.004 a.u.) at the PBE0-D4/def2-TZVP level of theory.

most electron-rich (nucleophilic) and electron-deficient (electrophilic) regions. As shown in Fig. 5, the highest positive MEP values are located on the hydrogen atoms of the coordinated amino groups (59.0 and 57.7 kcal mol^{-1}), as well as in the region influenced by both methyl groups of the coordinated DMSO ligand (55.2 kcal mol^{-1}). Significant positive potentials are also observed on the hydrogen atoms of the aliphatic linker between the amino groups (37.7 kcal mol^{-1}) and on the hydrogen atoms of the coordinated water molecule (38.9 and 46.4 kcal mol^{-1}). In contrast, the most negative MEP values are found on the thiocyanate ligands coordinated to the cobalt(II) center (−52.7 and −56.5 kcal mol^{-1}), followed by the thiocyanate ligand bound to the cobalt(III) center. These findings are consistent with the supramolecular assemblies depicted in Fig. 4 and support the structure-directing role of NH···S and OH···O hydrogen bonding interactions.

The QTAIM/NCIplot analysis of the assemblies is presented in Fig. 6. The OH···O(DMF) hydrogen bonds forming the $R_4^4(8)$ supramolecular ring are clearly identified by bond critical points (BCPs) and bond paths connecting the hydrogen and oxygen atoms. These hydrogen bonds are further visualized by blue reduced density gradient (RDG) isosurfaces, indicative of their strong and attractive nature. The calculated formation energy is substantial (−31.4 kcal mol^{-1}), highlighting the significance of this synthon in the solid-state architecture of the complex. The individual strengths of the hydrogen bonds are noted adjacent to the BCPs in Fig. 6a, showing a difference of 1.7 kcal mol^{-1}. This variation is consistent with the MEP analysis, which revealed distinct electrostatic potential values at the two hydrogen atoms of the coordinated water molecule.

The combined QTAIM/NCIplot analysis of the homodimer is presented in Fig. 6b. Four bond critical points (BCPs) and corresponding bond paths are observed, connecting the two monomeric units. Two of these correspond to NH···S hydrogen bonds, while the other two involve CH···S contacts between methyl hydrogen atoms and the sulfur atoms of the thiocyanate ligands. The NH···S interactions are characterized by small, disk-shaped RDG isosurfaces, typical of classical hydrogen bonds. In contrast, the CH···S contacts exhibit more extended RDG isosurfaces that encompass both the sulfur and carbon atoms of the SCN ligand, a shape more commonly associated with CH···π interactions. The directionality of these CH···S contacts suggests a significant contribution from the π-system of the thiocyanate acting as an electron donor. The interaction energy for the dimer is also notably large and negative (−30.1 kcal mol^{-1}), supporting the formation of infinite one-dimensional supramolecular chains in the solid state, stabilized by the combined effect of NH···S and CH···S interactions.

The theoretical results obtained at the PBE0-D4/def2-TZVP level show good agreement with the experimental observations. The spin density analysis confirms that the unpaired electron density is predominantly localized on the five-

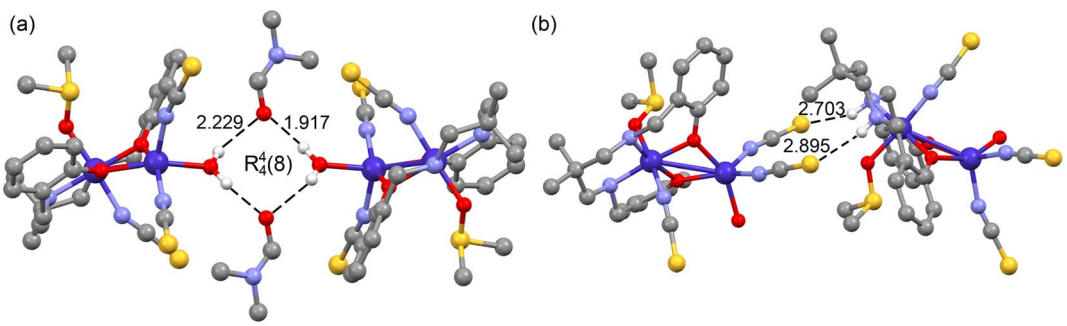

Fig. 4 Partial view of the tetrameric (a) and homodimeric (b) assemblies observed in the solid state of the complex. Distances in Å.

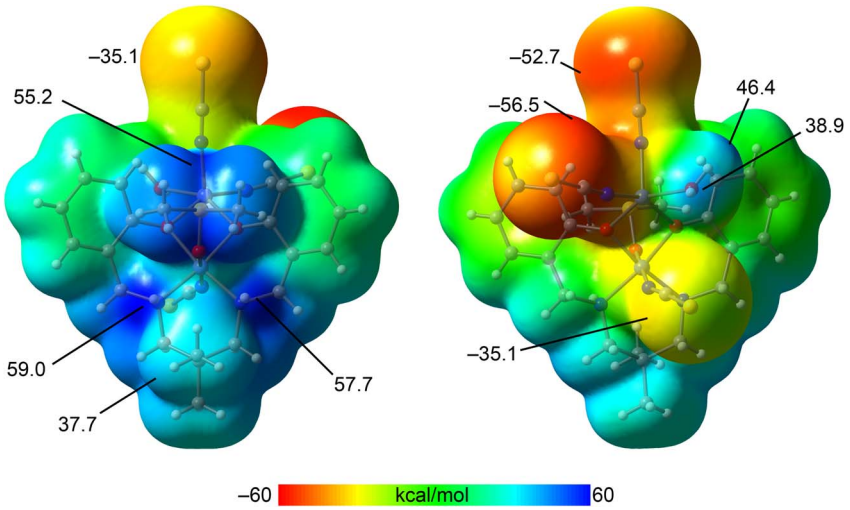

Fig. 5 Two views of the MEP surface of the complex. Energies at selected points of the surface are indicated in kcal mol^{-1}. Isovalue 0.001 a.u.

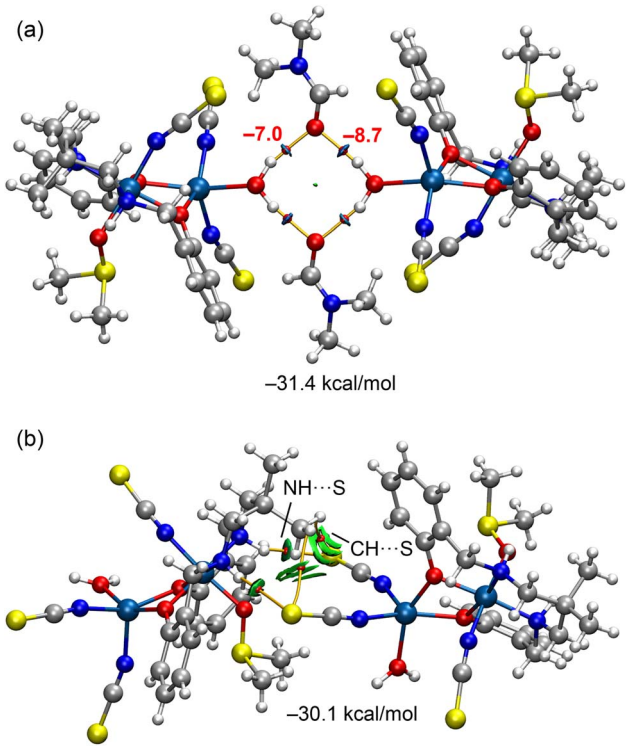

Fig. 6 QTAIM/NCIplot analysis of the tetramer (a) and the homodimer (b) of the complexes. The formation energies of the assemblies are also indicated.

coordinate Co(II) center, while the Co(III) center remains essentially diamagnetic, consistent with the bond length analysis derived from single-crystal X-ray diffraction. In addition, the DFT-calculated supramolecular assemblies reveal strong NH···S and OH···O hydrogen bonds, which match the key interactions identified in the crystal structure. The substantial calculated interaction energies (up to −31.4 kcal mol^{-1}) corroborate the importance of these contacts in stabilizing the extended one-dimensional network observed experimentally. Therefore, the theoretical findings not only support but also enhance the interpretation of the experimental structural data.

Conclusion

In summary, we have synthesized and structurally characterized a novel dinuclear cobalt(III/II) complex derived from a reduced Schiff base ligand. The complex features distinct coordination geometries around the cobalt centers, as confirmed by single-crystal X-ray diffraction. A detailed DFT study, including spin density mapping, molecular electrostatic potential (MEP) surfaces, and topological analyses (QTAIM and NCIplot), has provided valuable insights into the electronic distribution and the nature of the noncovalent interactions that stabilize the supramolecular architecture. The strong NH···S and OH···O hydrogen bonds, as well as weaker CH···S contacts, contribute significantly to the formation of extended 1D networks in the solid state. These results underscore the importance of combining experimental and theoretical approaches to understand the role of noncovalent forces in the assembly of mixed-valence coordination complexes and may guide future design of supramolecular materials with tailored properties.

Data availability

All data underlying the results are available as part of the article and no additional source data are required.

Conflicts of interest

There are no conflicts to declare.

Acknowledgements

S. Bera and S. Bhunia thank the UGC, India, for awarding Senior Research Fellowships. The authors are grateful to Projects

PID2020-115637GB-I00 and PID2023-148453NB-I00 funded by the Ministerio de Ciencia, Innovación y Universidades of Spain MCIU/AEI/10.13039/501100011033 and FEDER, UE.

Notes and references

1 P. Koley, B. Ghosh, J. Bhattacharyya and A. Hazari, *Mol. Catal.*, 2024, **569**, 114523.
2 L. K. Das, A. Biswas, J. S. Kinyon, N. S. Dalal, H. Zhou and A. Ghosh, *Inorg. Chem.*, 2013, **52**, 11744–11757.
3 J. Mandal, A. Dey, S. Sarkar, M. Khatun, P. Ghorai, P. P. Ray, P. Mahata and A. Saha, *Inorg. Chem.*, 2024, **63**, 4527–4544.
4 J. Mandal, P. Brandão, S. Benmansour, C. J. Gómez-García and A. Saha, *Cryst. Growth Des.*, 2022, **22**, 7544–7554.
5 H.-H. Zhang, Y.-B. Ren, Z.-L. Yuan, N.-X. Kang, S. Mehdi, C.-C. Xing, X.-Y. Liu, Y.-P. Fan, B.-J. Li and B.-Z. Liu, *Rare Met.*, 2023, **42**, 1935–1945.
6 Y. J. Lee and S. –K. Park, *Rare Met.*, 2024, **43**, 522–532.
7 J. Wu, Y. Zhang, Q. Hong, H. Yang, L. Zhang, M. Zhang and L. Yu, *Chin. Chem. Lett.*, 2025, **36**, 110165.
8 A. K. Ghosh, D. Ghoshal, E. Zangrando, J. Ribas and N. R. Chaudhuri, *Inorg. Chem.*, 2005, **44**, 1786–1793.
9 B. Santra, P. Kalita, S. Chandra, D. Mandal, V. Kumar, R. S. Narayanan, A. Dey, N. Chrysochos, V. Huch, S. Biswas, D. Ghoshal, E. C. Sañudo, B. Sarkar, C. Schulzke, V. Chandrasekhar and A. Jana, *Dalton Trans.*, 2020, **49**, 2527–2536.
10 M. Shit, M. Mahapatra, N. Sepay, C. Sinha, B. Dutta and M. H. Mir, *Chem.–Eur. J.*, 2024, **30**, e202402425.
11 S. Ahmed, D. Sahoo, P. Brandão, S. Bhunia, N. B. Manik and C. Sinha, *Inorg. Chim. Acta*, 2024, **572**, 122277.
12 S. S. Bera and M. Szostak, *ACS Catal.*, 2022, **12**, 3111–3137.
13 R. Debnath, P. Ghosh and S. Koner, *Appl. Organomet. Chem.*, 2025, **39**, e7815.
14 K. Das, T. N. Mandal, S. Roy, A. Jana, S. Konar, C.-M. Liu, A. K. Barik and S. K. Kar, *Polyhedron*, 2011, **30**, 715–724.
15 R. Sen, D. K. Hazra, S. Koner, M. Helliwell, M. Mukherjee and A. Bhattacharjee, *Polyhedron*, 2010, **29**, 3183–3191.
16 E. Zahradníková, C. Pichon, C. Duhayon, J.-P. Sutter, P. Halaš and B. Drahoš, *RSC Adv.*, 2024, **14**, 28138–28147.
17 I. Banerjee, A. Jana, S. Singh, J. Marek, E. d. Barco and M. Ali, *Polyhedron*, 2013, **66**, 162–166.
18 A. A. Pavlov, Y. V. Nelyubina, S. V. Kats, L. V. Penkova, N. N. Efimov, A. O. Dmitrienko, A. V. Vologzhanina, A. S. Belov, Y. Z. Voloshin and V. V. Novikov, *J. Phys. Chem. Lett.*, 2016, **7**, 4111–4116.
19 A. S. Belov, S. A. Belova, N. N. Efimov, V. V. Zlobina, V. V. Novikov, Y. V. Nelyubina, Y. V. Zubavichus, Y. Z. Voloshin and A. A. Pavlov, *Dalton Trans.*, 2023, **52**, 2928–2932.
20 S. A. Belova, A. S. Belov, A. A. Danshina, Y. V. Zubavichus, D. Y. Aleshin, A. A. Pavlov, N. N. Efimov and Y. Z. Voloshin, *Dalton Trans.*, 2024, **53**, 1482–1491.
21 N. Plyuta, S. Petrusenko, V. N. Kokozay, T. Cauchy, F. Lloret, M. Julve, J. Cano and N. Avarvari, *Dalton Trans.*, 2022, **51**, 4760–4771.
22 A. Zabala-Lekuona, A. Landart-Gereka, M. M. Quesada-Moreno, A. J. Mota, I. F. Díaz-Ortega, H. Nojiri, J. Krzystek, J. M. Seco and E. Colacio, *Inorg. Chem.*, 2023, **62**, 20030–20041.
23 S. S. Massoud, F. A. Mautner, H. Sakiyama, F. R. Louka, N. H. M. Salem, R. C. Fischer, A. Torvisco, T. Guizouarn and G. Velmurugan, *Eur. J. Inorg. Chem.*, 2025, e202400777.
24 J. G. McAlpin, T. A. Stich, W. H. Casey and R. D. Britt, *Coord. Chem. Rev.*, 2012, **256**, 2445–2452.
25 B. S. Brunschwig, M. H. Chou, Q. Creutz, P. Ghosh and N. Sutin, *J. Am. Chem. Soc.*, 1983, **105**, 4832–4833.
26 M. Schilling, G. R. Patzke, J. Hutter and S. Luber, *J. Phys. Chem. C*, 2016, **120**, 7966–7975.
27 M. M. Najafpour and H. Feizi, *Catal. Sci. Technol.*, 2018, **8**, 1840–1848.
28 D. S. Nesterov and O. V. Nesterova, *Catalysts*, 2018, **8**(12), 602.
29 A. Ray, G. M. Rosair, R. Kadam and S. Mitra, *Polyhedron*, 2009, **28**, 796–806.
30 T. G. Dastidar and S. Chattopadhyay, *Polyhedron*, 2022, **211**, 115511.
31 A. Hazari, L. K. Das, R. M. Kadam, A. Bauzá, A. Frontera and A. Ghosh, *Dalton Trans.*, 2015, **44**, 3862–3876.
32 E. Evangelio, N. P. Rath and L. M. Mirica, *Dalton Trans.*, 2012, **41**, 8010–8021.
33 Y.-C. Su, C.-Y. Tsai, L.-S. Huang, C.-H. Lin and B.-T. Ko, *Dalton Trans.*, 2019, **48**, 12239–12249.
34 S. Dutta, P. Biswas, U. Florke and K. Nag, *Inorg. Chem.*, 2010, **49**, 7217–7219.
35 Z.-L. You, *Acta Crystallogr.*, 2005, **C61**, m295.
36 J. Tang, F. Huang, Y. Wei, H. Bian, W. Zhang and H. Liang, *Dalton Trans.*, 2016, **45**, 8061–8072.
37 Z.-L. You, D.-H. Shi, C. Xu, Q. Zhang and H.-L. Zhu, *Eur. J. Med. Chem.*, 2008, **43**, 862–871.
38 R. S. Sarkar, S. Banerjee and S. Chattopadhyay, *Polyhedron*, 2024, **254**, 116916.
39 D.-H. Shi, Z.-L. You, C. Xu, Q. Zhang and H.-L. Zhu, *Inorg. Chem. Commun.*, 2007, **10**, 404–406.
40 X. He, C.-Z. Lu and C.-D. Wu, *J. Coord. Chem.*, 2006, **59**, 977–984.
41 C. Fukuhara, E. Asato, T. Shimoji and K. Katsura, *J. Chem. Soc., Dalton Trans.*, 1987, 1305–1311.
42 A. Banerjee, S. Banerjee, C. J. G. Garcia, S. Benmansour and S. Chattopadhyay, *Dalton Trans.*, 2020, **49**, 16778–16790.
43 A. Banerjee, C. J. G. Garcia, S. Benmansour, R. M. Gomila, A. Frontera and S. Chattopadhyay, *Polyhedron*, 2022, **220**, 115802.
44 A. Banerjee, D. Das, P. P. Ray, S. Banerjee and S. Chattopadhyay, *Dalton Trans.*, 2021, **50**, 1721–1732.
45 S. Bhunia, M. Das, S. Banerjee, M. G. B. Drew, P. P. Ray and S. Chattopadhyay, *RSC Adv.*, 2024, **14**, 11185–11196.
46 R. S. Sarkar, A. Biswas, P. P. Ray, R. M. Gomila, M. G. B. Drew, S. Banerjee, A. Frontera and S. Chattopadhyay, *CrystEngComm*, 2023, **25**, 1006–1017.
47 A. Hazari, A. Das, P. Mahapatra and A. Ghosh, *Polyhedron*, 2017, **134**, 99–106.

48 A. Banerjee and S. Chattopadhyay, *Polyhedreon*, 2020, **177**, 114290.
49 K. Ghosh, M. G. B. Drew and S. Chattopadhyay, *Inorg. Chim. Acta*, 2018, **482**, 23–33.
50 K. Ghosh, S. Roy, A. Ghosh, A. Banerjee, A. Bauza, A. Frontera and S. Chattopadhyay, *Polyhedron*, 2016, **112**, 6–17.
51 K. Ghosh, K. Harms and S. Chattopadhyay, *ChemistrySelect*, 2017, **2**, 8207–8220.
52 K. Ghosh, K. Harms, A. Franconetti, A. Frontera and S. Chattopadhyay, *J. Organomet. Chem.*, 2019, **883**, 52–64.
53 S. Roy, M. G. B. Drew, A. Bauzá, A. Frontera and S. Chattopadhyay, *Dalton Trans.*, 2017, **46**, 5384–5397.
54 S. Tsuzuki and A. Fujii, *Phys. Chem. Chem. Phys.*, 2008, **10**, 2584–2594.
55 T.-H. Huang and M.-H. Zhang, *Inorg. Chim. Acta*, 2014, **416**, 28–34.
56 B. Mirtamizdoust, A. Karamad, F. Mojtabazade, H. Hosein-Monfared, R. Bikas, Z. Zák, H. Erfani, S. Jadoun and A. K. Mishra, *ACS Omega*, 2024, **9**, 5563–5575.
57 M. Nishio, *CrystEngComm*, 2004, **6**, 130–158.
58 M. Bazargan, M. Mirzaei, A. S. Hamid, Z. H. Kafshdar, H. Ziaekhodadadian, E. Momenzadeh, J. T. Mague, D. M. Gil, R. M. Gomila and A. Frontera, *CrystEngComm*, 2022, **24**, 6677–6687.
59 U. Mukhopadhyay, D. Choquesillo-Lazarte, J. Niclós-Gutiérrez and I. Bernal, *CrystEngComm*, 2004, **6**, 627–632.
60 A. M. Keys, D. W. Kastner, L. L. Kiessling and H. J. Kulik, *Chem. Sci.*, 2025, **16**, 1746–1761.
61 R. Gaur, S. Roy, P. Kallem and F. Banat, *J. Mol. Struct.*, 2022, **1265**, 133400.
62 P. K. Bhaumik, A. Frontera and S. Chattopadhyay, *Inorg. Chim. Acta*, 2021, **515**, 120023.
63 Y. V. Torubaev, D. K. Rai, I. V. Skabitsky, S. Pakhira and A. Dmitrienko, *New J. Chem.*, 2019, **43**, 7941–7949.
64 F. Biedermann and H.-J. Schneider, *Chem. Rev.*, 2016, **116**, 5216–5300.
65 N. Bäumer, K. K. Kartha, S. Buss, I. Maisuls, J. P. Palakkal, C. A. Strassert and G. Fernández, *Chem. Sci.*, 2021, **12**, 5236–5245.
66 A. N. Malik, M. N. Tahir, A. Ali, M. Ashfaq, M. Ibrahim, A. E. Kuznetsov, M. A. Assiri and M. Y. Sameeh, *ACS Omega*, 2023, **8**, 25034–25047.
67 J. Antony, R. Sure and S. Grimme, *Chem. Commun.*, 2015, **51**, 1764–1774.
68 G. M. Sheldrick, *Acta Crystallogr., Sect. C: Struct. Chem.*, 2015, **71**, 3.
69 G. M. Sheldrick, *Sadabs, V2014/5, Software for Empirical Absorption Correction*, University of Göttingen, Institute fur Anorganische Chemie der Universitat, Gottingen, Germany, 1999.
70 M. A. Spackman and D. Jayatilaka, *CrystEngComm*, 2009, **11**, 19–32.
71 H. F. Clausen, M. S. Chevallier, M. A. Spackman and B. B. Iversen, *New J. Chem.*, 2010, **34**, 193–199.
72 A. L. Rohl, M. Moret, W. Kaminsky, K. Claborn, J. J. McKinnon and B. Kahr, *Cryst. Growth Des.*, 2008, **8**, 4517–4525.
73 C. Adamo and V. Barone, *J. Chem. Phys.*, 1999, **110**, 6158–6170.
74 F. Weigend and R. Ahlrichs, *Phys. Chem. Chem. Phys.*, 2005, **7**, 3297–3305.
75 S. Grimme, J. Antony, S. Ehrlich and H. Krieg, *J. Chem. Phys.*, 2010, **132**, 154104.
76 R. Ahlrichs, M. Bär, M. Hacer, H. Horn and C. Kömel, *Chem. Phys. Lett.*, 1989, **162**, 165–169.
77 R. F. W. Bader, *Chem. Rev.*, 1991, **91**, 893–928.
78 E. R. Johnson, S. Keinan, P. Mori-Sánchez, J. Contreras-García, A. J. Cohen and W. Yang, *J. Am. Chem. Soc.*, 2010, **132**, 6498–6506.
79 T. Lu and F. Chen, *J. Comput. Chem.*, 2012, **33**, 580–592.
80 D. Coskun, S. V. Jerome and R. A. Friesner, *J. Chem. Theory Comput.*, 2016, **12**, 1121–1128.
81 W.-J. Lian, X.-T. Wang, C.-Z. Xie, H. Tian, X.-Q. Song, H.-T. Pan, X. Qiao and J.-Y. Xu, *Dalton Trans.*, 2016, **45**, 9073–9087.
82 P. Middya, S. D. Sarkar and S. Chattopadhyay, *J. Mol. Struct.*, 2025, **1322**, 140242.
83 S. Bhunia and S. Chattopadhyay, *Inorg. Chim. Acta*, 2025, **577**, 122475.
84 R. S. Sarkar, C. J. G. García, S. Benmansour and S. Chattopadhyay, *Polyhedron*, 2025, **269**, 117425.
85 J. Welby, L. N. Rusere, J. M. Tanski and L. A. Tyler, *Inorg. Chim. Acta*, 2009, **362**, 1405–1411.
86 E. Baca-Solis, S. Bern'es, H. Vazquez-Lima, M.-E. Boulon, R. E. P. Winpenny and Y. Reyes-Ortega, *ChemistrySelect*, 2016, **1**, 6866–6871.
87 X. He, C.-Z. Lu and C.-D. Wu, *J. Coord. Chem.*, 2006, **59**, 977–984.
88 A. D. Khalaji and S. Triki, *Russ. J. Coord. Chem.*, 2011, **37**, 664–667.
89 S. Banerjee, M. Nandy, S. Sen, S. Mandal, G. M. Rosair, A. M. Z. Slawin, C. J. G. Garcia, J. M. Clemente-Juan, E. Zangrando, N. Guidolin and S. Mitra, *Dalton Trans.*, 2011, **40**, 1652–1661.
90 S. Bera, S. Bhunia, R. M. Gomila, M. G. B. Drew, A. Frontera and S. Chattopadhyay, *RSC Adv.*, 2023, **13**, 29568–29583.
91 D. Cremer, *Acta Crystallogr., Sect. B: Struct. Sci.*, 1984, **40**, 498–500.
92 J. C. A. Boeyens, *J. Cryst. Mol. Struct.*, 1978, **8**, 317–320.
93 T. Basak, S. Roy, S. Banerjee and S. Chattopadhyay, *Inorg. Chim. Acta*, 2022, **543**, 121186.
94 S. Roy, B. Halder, R. M. Gomila, A. Frontera, M. G. B. Drew and S. Chattopadhyay, *Inorg. Chim. Acta*, 2024, **573**, 122323.
95 S. Bera, A. Frontera and S. Chattopadhyay, *Polyhedron*, 2025, **14**, 117422.
96 S. Chattopadhyay, M. S. Ray, S. Chaudhuri, G. Mukhopadhyay, G. Bocelli, A. Cantoni and A. Ghosh, *Inorg. Chim. Acta*, 2006, **359**, 1367–1375.
97 A. Bhattacharyya, M. Das, A. Bauza, S. Herrero, R. G. Prieto, A. Frontera and S. Chattopadhyay, *New J. Chem.*, 2017, **41**, 13585–13592.

98 A. Ray, G. M. Rosair, G. Pilet, B. Dede, C. J. Gomez-García, S. Signorella, S. Bellú and S. Mitra, *Inorg. Chim. Acta*, 2011, **375**, 20–30.
99 H. A. R. Pramanik, P. C. Paul, P. Mondal and C. R. Bhattacharjee, *J. Mol. Struct.*, 2015, **1100**, 496–505.
100 S. Bhunia, M. Das, S. Banerjee, M. G. B. Drew, P. P. Ray and S. Chattopadhyay, *RSC Adv.*, 2024, **14**, 11185–11196.
101 M. Das and S. Chattopadhyay, *Polyhedron*, 2013, **50**, 443–451.